Electronic structures and spin states of $BaFe_2As_2$ and $SrFe_2As_2$ probed by x-ray emission spectroscopy at Fe and As K-absorption edges

Hitoshi Yamaoka,[1,*] Yoshiya Yamamoto,[2] Jung-Fu Lin,[3,4] Junjie J. Wu,[3,4] Xiancheng Wang,[5] Changqing Jin,[5] Masahiro Yoshida,[2,†] Seiichiro Onari,[6] Shigeyuki Ishida,[7] Yoshinori Tsuchiya,[7] Nao Takeshita,[7] Nozomu Hiraoka,[8] Hirofumi Ishii,[8] Ku-Ding Tsuei,[8] Paul Chow,[9] Yuming Xiao,[9] and Jun'ichiro Mizuki[2]

[1]*RIKEN SPring-8 Center, 1-1-1 Kouto, Mikazuki, Sayo, Hyogo 679-5148, Japan*

[2]*Graduate School of Science and Technology, Kwansei Gakuin University, Sanda, Hyogo 669-1337, Japan*

[3]*Department of Geological Sciences, The University of Texas at Austin, Austin, Texas 78712, USA*

[4]*Center for High Pressure Science and Technology Advanced Research (HPSTAR), Shanghai 201203, China*

[5]*Institute of Physics, Chinese Academy of Sciences, School of Physics, University of Chinese Academy of Sciences, Beijing 100190, China*

[6]*Department of Physics, Okayama University, Okayama 700-8530, Japan*

[7]*National Institute of Advanced Industrial Science and Technology (AIST), Tsukuba, Ibaraki 305-8562, Japan*

[8]*National Synchrotron Radiation Research Center, Hsinchu 30076, Taiwan*

[9]*HPCAT, Geophysical Laboratory, Carnegie Institution of Washington, Argonne, Illinois 60439, USA*

(Received 25 June 2017; revised manuscript received 24 July 2017; published 22 August 2017)

Electronic structures of electron- and hole-doped $BaFe_2As_2$ and nondoped $SrFe_2As_2$ have been studied systematically by x-ray emission spectroscopy at Fe and As K-absorption edges. The electron and hole doping causes slight increase of the integrated absolute difference (IAD) values of the Fe $K\beta$ x-ray emission spectra which correlate to the local magnetic moment. Pressure decreases the IAD values and local magnetic moment, and induces the lower-spin states in these compounds. The pre-edge peak intensity of the XAS spectra at the Fe K-absorption edge increases with pressure in both compounds. This indicates an increase of the Fe $3d$–As $4p$ hybridization. It was found that pressure induced a discontinuous increase of the prepeak intensity of the PFY-XAS spectra at the As K-absorption edge at low pressures in the $BaFe_2As_2$ systems. Our results may suggest that the Fe $3d$–As $4p$ hybridization plays a key role in suppressing the AFM order by the doping or pressure and fluctuation of the local magnetic moment and the electron-electron correlation may also play a role on the physical properties of the iron superconductors.

DOI: 10.1103/PhysRevB.96.085129

I. INTRODUCTION

High-temperature superconductivity in F-doped LaFeAsO was found in 2008 (Ref. [1]) and many iron-based superconductors with different crystal structures have been synthesized [2,3]. Most iron-superconductor families have FeAs or FeSe planes as the common layers, which correlate to the superconductivity. The Fe-As-Fe angle or pnictogen height is an important parameter crystallographically. It correlates to the superconducting transition temperature (T_c) [4–7]. Although superconductivity and magnetism had been considered to compete against each other, non-BCS-type high-T_c superconductors show a close relation between magnetism and superconductivity. Theoretically it is suggested that the pairing interaction is mediated by exchange of the antiferromagnetic (AFM) spin fluctuations, where the pairing is due to the hopping of electrons between the electron and hole pockets, or by the orbital fluctuations [3,8,9].

Thus in iron-based superconductors AFM correlation is one of the most important concerns because the region of the AFM order often merges into the superconducting dome in the phase diagram. It is known that in the nondoped parent compounds the ordered magnetic moment is much smaller than the local moment. This suggests that the local magnetic moment strongly fluctuates and the residual moment remains ordered [10]. Therefore, the magnetic fluctuation may play an important role on the physical properties of the iron superconductors. Recent theoretical calculations using a spin-fermion model with ferromagnetic Hund's coupling showed that the itinerant carriers with well-nested Fermi surfaces were found to induce a spatial and temporal quantum fluctuation, leading to the observed small ordered moment [10]. The underlying mechanism was an intrapocket nesting-associated long-range coupling rather than the ferromagnetic double-exchange effect.

The ternary 122-type AFe_2As_2 (A = Eu, Ca, Sr, and Ba) compounds exhibit a temperature-induced tetragonal-to-orthorhombic structural transition strongly coupled with a paramagnetic-to-antiferromagnetic transition with decreasing temperature. AFe_2As_2 does not show superconductivity at ambient pressure. In $BaFe_2As_2$ electron doping, hole doping, and pressure suppress the AFM order and induce superconductivity. The pressure-induced structural transition from the tetragonal (T) to the collapsed tetragonal (cT) phase is a universal characteristic of AFe_2As_2 compounds [11–17]. Some theoretical studies focused mainly on the interlayer As-As distance under pressure [18–20]. It was suggested that the spin state of Fe is one of the key parameters that controls As-As bonding and, consequently, the lattice parameters [19]. In $BaFe_2As_2$ a small amount of the electron doping of Co atoms to the Fe sites does not change the lattice parameters much [21]. However, the hole doping of K atoms to the Ba sites causes the lattice parameter of a to decrease and that of c to increase

*Corresponding author: yamaoka@spring8.or.jp

†Present address: Institute of Solid State Physics, The University of Tokyo, 5-1-5 Kashiwanoha, Kashiwa, Chiba 277-8581, Japan.

monotonically [22,23]. In $BaFe_2As_2$ the As-Fe-As bond angle is about 111° which is larger than the ideal tetrahedral bond angle of 109.47°. The ideal tetrahedral bond angle corresponds to the K-doping content of $x = 0.3$–0.5 in $Ba_{1-x}K_xFe_2As_2$, where high T_c was observed. The pressure-temperature phase diagram of $BaFe_2As_2$ has been studied by x-ray diffraction and synchrotron Mössbauer spectroscopy (SRS) under pressure [24]. The results suggested that Fe^{+2} exhibits mesoscopic spin moments right before the structural transition decreases in temperature and the local moments involving the fluctuation although the nematic phase was not detectable due to the problem of the time scale of SRS. Interaction of the electron spins, thus, plays a role in the origin of superconductivity in pnictides. However, the spin states of the doped systems of AFe_2As_2 have still not been explored systematically.

An x-ray absorption spectroscopy (XAS) study was performed at the Fe-K edge for the hole-doped system of $Ba(Fe_{1-y}Co_y)_2As_2$ [25]. The XAS spectra did not show a remarkable change through the temperature-induced phase transitions, but pressure lead to slight energy shift of the main edge not the pre-edge. However, XAS at the As K edge showed the strong sensitivity of the As electronic structure upon electron doping with Co or pressure change in $BaFe_2As_2$ at room temperature [26]. These results indicated the prominent role of the As-4p orbitals in the electronic properties of the Fe pnictide superconductors. These studies motivate us to perform a systematic x-ray spectroscopy study by extending the systems to not only the hole-doped $BaFe_2As_2$, but also the electron-doped $BaFe_2As_2$ and $SrFe_2As_2$ at the Fe and As K-absorption edges. A systematic study of the electronic structures of the doped $BaFe_2As_2$ and $SrFe_2As_2$ has been reported by XAS at $L_{2,3}$ absorption edge [27,28]. Although the shift in the energy position of the L_3 edge observed maximum peak, the study indicated that the doping plays a lesser role for pnictide superconductivity and magnetism. We note that the XAS study at the Fe and As K-absorption edges was advantageous because we now know the spin state and the d-p hybridization, respectively.

A pressure-temperature phase diagram of the crystal structure of $SrFe_2As_2$ is similar to that of $BaFe_2As_2$ [29,30]. The detailed XRD study indicated that the paramagnetic to antiferromagnetic and tetragonal to orthorhombic structural transitions were coupled at 205 K at ambient pressure, and two transitions were concurrently suppressed to much lower temperatures near a quantum critical pressure of approximately 4.8 GPa where the antiferromagnetic state transforms into a bulk superconducting state [31]. This suggested that both the lattice distortions and magnetism strongly correlated to the appearance of the superconductivity under pressure. The T $\rightarrow$ cT structural transition was observed around 10 GPa at room temperature [15,32]. The nuclear resonant inelastic x-ray scattering showed that the partial density of states of $SrFe_2As_2$ changed dramatically at approximately 8 GPa. This could be associated with the T $\rightarrow$ cT isostructural transition [32].

In $BaFe_2As_2$ and $SrFe_2As_2$ no superconductivity has been observed; however, the chemical substitution or pressure induced the superconductivity. The electronic structure including the spin state as well as the crystal structure may play an important role in the emergence of superconductivity. In this paper we report a systematic study of the chemical composition dependence of the electronic structures and spin states of electron- and hole-doped $BaFe_2As_2$: $Ba_{1-x}K_xFe_2As_2$ and $Ba(Fe_{1-y}Co_y)_2As_2$. Pressure could tune superconducting states without introducing local disorder in comparison to chemical doping. We also study pressure-induced change in the electronic structure of $BaFe_2As_2$ and $SrFe_2As_2$. We employ the Fe and As $K\beta$ x-ray emission spectroscopy (XES) as a bulk-sensitive probe of the electronic structure. The XES method allows us to study the electronic structure under pressure, where the photoelectron spectroscopy cannot be applicable. It is known that the Fe $K\beta$ spectrum consists of two components of a strong $K\beta_{1,3}$ component and a weak satellite of $K\beta'$ component, corresponding to mainly low-spin and high-spin state, respectively [33,34]. Change in the intensity of the Fe $K\beta$ spectra, so-called integrated absolute difference (IAD) value, is a measure of spin state as well as the magnetic moment [19,35–37]. The x-ray absorption spectra with partial fluorescence yield mode (PFY-XAS) [38–40] were also measured. The pre-edge, prepeak, and shoulder structures at the absorption edge of the PFY-XAS spectra reflect the hybridization strength of Fe 3d and As 4p. In Fe-based superconductors it has been considered that Fe d electrons play an important role through the orbital fluctuations for the emergence of the superconductivity. We emphasize that it is an advantage that we could know the electronic state of Fe d electrons from the pre-edge peak of the XAS spectra at the Fe-K absorption edge.

II. EXPERIMENTS AND METHODS

High-quality single crystals and polycrystals of $Ba_{1-x}K_xFe_2As_2$, $Ba(Fe_{1-y}Co_y)_2As_2$, and $SrFe_2As_2$ were prepared. The results of the XRD in Figs. 2(d) and 2(e) and the PFY-XAS spectra in Figs. 6–8 at the As K-absorption edge were the data for the polycrystals and the other results were for the single crystals. Polycrystalline samples of $Ba_{1-x}K_xFe_2As_2$ were annealed 24 or 48 h at 790–850 °C and those of $Ba(Fe_{1-y}Co_y)_2As_2$ were annealed at 880–900 °C. X-ray diffraction study was performed for the polycrystalline samples of the Ba122 systems using a laboratory x-ray source. The $SrFe_2As_2$ single crystals were grown using the self-flux method [41].

Measurements of the PFY-XAS and XES were performed at the Taiwan beamline BL12XU, SPring-8 [42,43] and at 16-ID-D beamline of the APS, ANL. At BL12XU of the SPring-8 the undulator beam was monochromatized by a cryogenically cooled double crystal Si(111) monochromator. A Johann-type spectrometer equipped with spherically bent analyzer crystals (radius of ~1 m) of Si(531) for Fe $K\beta$ emission and Si(844) for As $K\beta$ emission. A Si solid state detector (Amptech) was used to analyze the Fe emission of the $3p \rightarrow 1s$ deexcitation at the Fe and As K-absorption edges. We used the $K\beta$ emission of As, instead of the $K\alpha$ emission [26], because the As 3p electrons may be more correlative to the outer shell electrons compared to the 2p electrons. At the emitted photon energy of 7.6 keV the overall energy resolution was estimated to be 0.9 eV. Here, it is noted that one can discuss the relative change in the energy on the order of 0.1 eV, which is one order of magnitude as small as the energy spread of the analyzer. The intensities of the measured spectra were normalized

using the incident beam that was monitored just before the sample.

For the high-pressure experiments in the x-ray emission spectroscopy at SPring-8 the x-ray beam was focused to 20–30 (horizontal) × 30–40 (vertical) μm^2 at the sample position using a toroidal and a Kirkpatrick-Baez mirror. High-pressure conditions were achieved at room temperature using a diamond anvil cell coupled with a gas membrane. A Be-gasket 3 mm in diameter and approximately 100 μm thick was preindented to approximately 35–40 μm thickness around the center. The diameter of the sample chamber in the gasket was approximately 100–120 μm and the diamond anvil culet size was 300 μm. Pressure medium of Daphne oil was used for the DAC. We used the Be gasket in-plane geometry with a scattering angle of 90°, where both incoming and outgoing x-ray beams passed through the Be gasket. Pressure was monitored by the ruby fluorescence method [44–46]. We performed high-pressure experiments to find the pressure range where superconductivity appears and further pressure beyond.

Measurements of the PFY-XAS at the Fe K-absorption edge and Fe-$K\beta$ XES for $SrFe_2As_2$ were performed at 16-ID-D, APS. An incident x-ray beam with a beam size of 30 (vertical) × 50 (horizontal) μm^2 in diameter (FWHM) was used for the experiments. The incident x ray was focused onto the sample through one of the diamond anvils, and the Fe $K\beta$ emission spectra were collected by a silicon detector through the Be gasket and a Si(444) analyzer in the 1 m Rowland circle vertical geometry with a step size equivalent to about 0.3 eV. We used a 4 in. Si (333) analyzer to measure the PFY-XAS spectra at Fe $K\alpha_1$ peak. Pressure medium of Ne was used for the DAC.

The IAD analysis of the $K\beta$ XES spectra is performed in the following way: (i) match the center of mass between the sample and reference spectra exactly, (ii) take the difference between them, and (iii) integrate the absolute value of the difference. The intensity is normalized by the area of the $K\beta$ spectrum. The error of the IAD values and the pre-edge peak intensity mainly comes from the statistics of the total counts and fit errors. We increased statistics, especially for the $K\beta$ emission spectra because of the small change in the intensity.

Figure 1 shows the phase diagrams of $BaFe_2As_2$ and $SrFe_2As_2$ with the points measured. In the doped $BaFe_2As_2$ we study the doping, chemical composition, and pressure dependences of the electronic structure. In $SrFe_2As_2$ pressure dependence of the electronic structure at 17 and 300 K were measured.

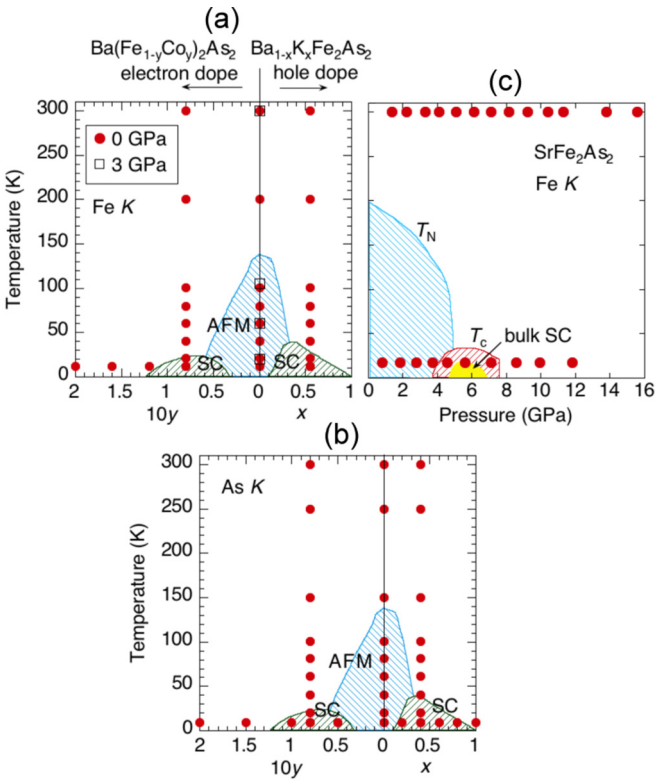

FIG. 1. (a) Phase diagram of $Ba(Fe_{1-y}Co_y)_2As_2$ and $Ba_{1-x}K_xFe_2As_2$ with the points where the XES and XAS measurements around the Fe K-absorption edges [21,22]. (b) The same phase diagram as (a) with the measured points at the As K-absorption edge. (c) A P-T phase diagram of $SrFe_2As_2$ with the measured points around the Fe K-absorption edge [30,31].

III. RESULTS

A. $BaFe_2As_2$

1. Fe $K\beta$ XES

Chemical composition dependence of the $K\beta$ XES spectra of $Ba(Fe_{1-y}Co_y)_2As_2$ and $Ba_{1-x}K_xFe_2As_2$ at 12 K is shown in Fig. 2(a) with a reference spectrum of FeCrAs; the change in the spectra seems to be small. While in $BaFe_2As_2$ pressure changes the spectra slightly at low temperatures as shown in Fig. 2(b). Chemical composition dependence of the IAD values are estimated for a reference spectrum of FeCrAs, which is known to have a low-spin state without magnetic moment [36], as shown in Fig. 2(c). Additionally, we show the chemical composition dependence of the lattice constants measured for the sample here (closed symbols) with the data taken from the literature (open symbols) [21,23] in Fig. 2(d). The ratio of the lattice constants a to c is plotted in Fig. 2(e). Present data of the lattice constants and the ratio show good agreement with the previous data. The ratio seems not to show anomalous features. It is noted that the change in the lattice constant in the Co substitution is very small, $\Delta a \sim 0.002$ Å, $\Delta c \sim 0.06$ Å, while in the K substitution $\Delta a \sim 0.115$ Å, $\Delta c \sim 0.8$ Å in the measured substitution range. Both the electron and hole doping to $BaFe_2As_2$ show a trend of increase in the IAD values.

Temperature dependence of the $K\beta$ XES spectra of $BaFe_2As_2$ at 0 GPa, $BaFe_2As_2$ at 3 GPa, $Ba(Fe_{0.92}Co_{0.08})_2As_2$ at 0 GPa, and $Ba_{0.45}K_{0.55}Fe_2As_2$ at 0 GPa are shown in Figs. 3(a)–3(d). The $y = 0.08$ and $x = 0.55$ samples correspond to the compositions where T_c takes a maximum. Temperature dependence of the IAD values are summarized in Fig. 3(e). At ambient pressure the IAD values of $Ba(Fe_{0.92}Co_{0.08})_2As_2$ and $Ba_{0.45}K_{0.55}Fe_2As_2$ decrease slightly with decreasing the temperature.

The pressure decreases the IAD value in $BaFe_2As_2$ at 300 K as shown in Fig. 3(e). This result is consistent with the previous ones where pressure induced the spin state from higher- to lower-spin states [43,47]. In $BaFe_2As_2$ the

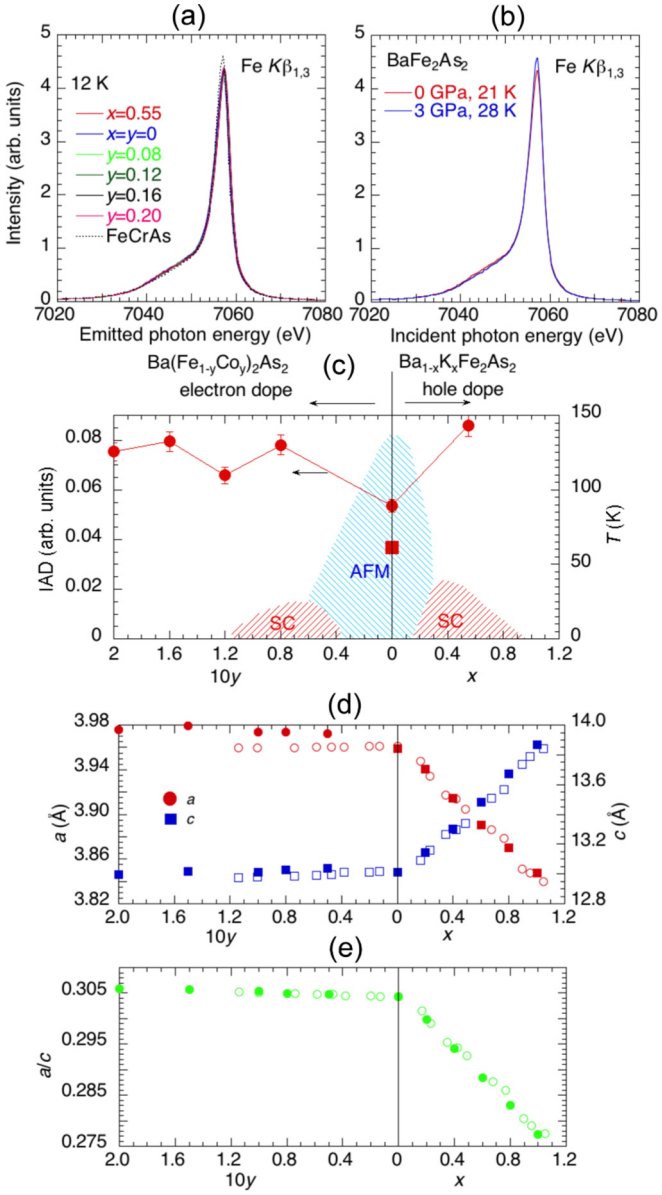

FIG. 2. (a) $K\beta$ x-ray emission spectra of $Ba(Fe_{1-y}Co_y)_2As_2$ and $Ba_{1-x}K_xFe_2As_2$ with a reference spectrum of FeCrAs. (b) Those of $BaFe_2As_2$ at 0 and 3 GPa. (c) The IAD values (left vertical axis) of $Ba(Fe_{1-y}Co_y)_2As_2$ and $Ba_{1-x}K_xFe_2As_2$ with the phase diagram. Closed circle and closed square correspond to the measurement at 0 and 3 GPa, respectively. Note that the horizontal scale of y is multiplied by a factor of 10. (d) The lattice constants of $Ba(Fe_{1-y}Co_y)_2As_2$ and $Ba_{1-x}K_xFe_2As_2$, where closed and open symbols correspond to the data taken in these experiments and from the literature, respectively [21,23]. (e) The ratio of the lattice constants a to c, where closed and open symbols are present and previous data, respectively.

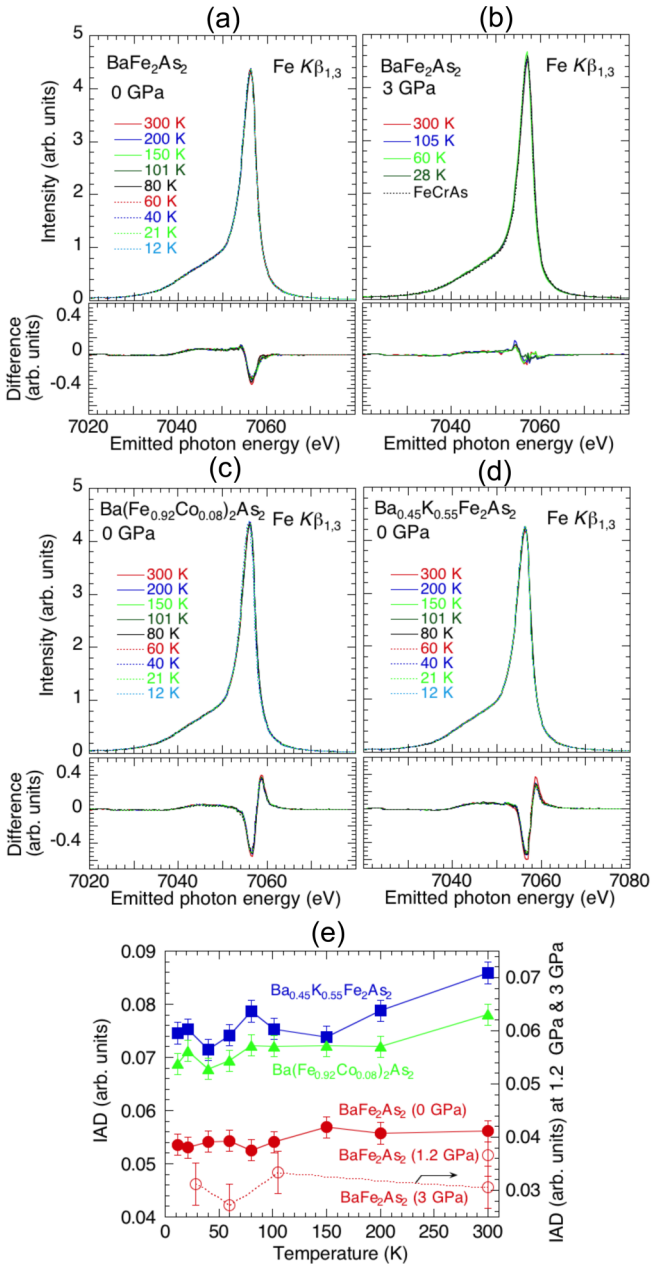

FIG. 3. Temperature dependence of the XES spectra of (a) $BaFe_2As_2$ at 0 GPa, (b) $BaFe_2As_2$ at 3 GPa, (c) $Ba(Fe_{0.92}Co_{0.08})_2As_2$ at 0 GPa, and (d) $Ba_{0.45}K_{0.55}Fe_2As_2$ at 0 GPa with the difference for a reference spectrum of FeCrAs (lower panels in each figure). Temperature dependence of the IAD values are shown in (e).

temperature-induced change in the IAD values are not clearly observed at 3 GPa, where the superconductivity observed.

2. *PFY-XAS at Fe K-absorption edge*

Chemical composition and pressure dependences of the PFY-XAS spectra are shown in Figs. 4(a) and 4(b), respectively. A fit example of the PFY-XAS spectrum of $BaFe_2As_2$ at 12 K is shown in Fig. 4(c), assuming two components of the pre-edge peak [48] and other components with an arctanlike background for simplicity. The pre-edge peak intensity and the ratio of the two components are shown in Fig. 4(d). The intensity of the pre-edge peak of the doped samples at $x = 0.5$ and $y > 0.12$ is larger than that of nondoped $BaFe_2As_2$. However, the chemical composition dependence of the pre-edge peak intensity and the ratio is not clear. On the other hand, pressure increases the intensity of the pre-edge peak largely, suggesting the increase of the p-d hybridization.

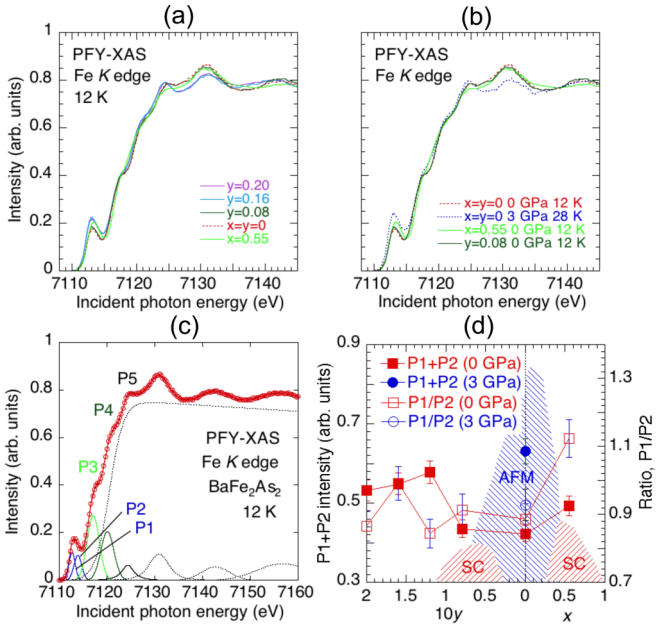

FIG. 4. (a) Chemical composition dependence of the PFY-XAS spectra at 12 K and 0 GPa. (b) PFY-XAS spectra of $BaFe_2As_2$ at 0 and 3 GPa and those of $Ba(Fe_{0.92}Co_{0.08})_2As_2$ at 0 GPa and $Ba_{0.45}K_{0.55}Fe_2As_2$ at 0 GPa. (c) A fit example of the PFY-XAS spectrum of $BaFe_2As_2$ at 12 K. (d) Chemical composition dependences of the pre-edge peak intensity and the intensity ratio of P1 to P2. A schematic figure of two superconducting and AFM regions are also shown, where the full vertical scale corresponds to 150 K [21,23].

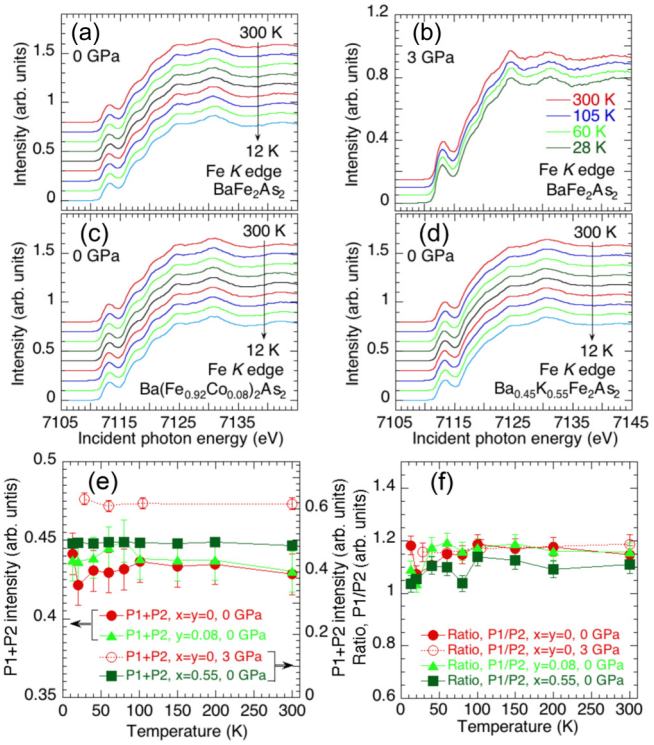

FIG. 5. (a)–(d) Temperature dependence of the PFY-XAS spectra of (a) $BaFe_2As_2$ at 0 GPa, (b) $BaFe_2As_2$ at 3 GPa, (c) $Ba(Fe_{0.92}Co_{0.08})_2As_2$ at 0 GPa, and (d) $Ba_{0.45}K_{0.55}Fe_2As_2$ at 0 GPa. (e) Temperature dependence of the pre-edge peak intensity. (f) Temperature dependence of the pre-edge peak intensity ratio of P1 to P2.

Temperature dependence of the PFY-XAS spectra at Fe K-absorption edge of $BaFe_2As_2$ at 0 GPa, $BaFe_2As_2$ at 3 GPa, $Ba(Fe_{0.92}Co_{0.08})_2As_2$ at 0 GPa, and $Ba_{0.45}K_{0.55}Fe_2As_2$ at 0 GPa are shown in Figs. 5(a)–5(d), respectively. Temperature dependence of the intensity of the pre-edge peak and the ratio are shown in Figs. 4(e) and 4(f). No significant temperature dependence of the PFY-XAS spectra is observed. Our results agree with those for $BaFe_2As_2$ and $Ba(Fe_{0.935}Co_{0.065})_2As_2$ previously measured by Balédent *et al.* [25].

3. *PFY-XAS at As K-absorption edge*

We performed As $K\beta$ x-ray emission spectroscopy and measured the PFY-XAS spectra at the As K-absorption edge because the above $K\beta$ x-ray emission spectra as well as the PFY-XAS spectra at the Fe K-absorption edge only show very small chemical composition and temperature dependences. Figure 6(a) shows the chemical composition dependence of the PFY-XAS spectra of $Ba(Fe_{1-y}Co_y)_2As_2$ and $Ba_{1-x}K_xFe_2As_2$ at the As K-absorption edge. The shift of the absorption edge energy is shown in Fig. 6(b) in $Ba_{1-x}K_xFe_2As_2$. The K doping to Ba site drastically induces the increase of the intensity of the prepeak around 11866 eV, lowering the absorption edge energy, and narrowing the width of the main peak around 11874 eV. This shift of the edge energy corresponds to lowering the charge state of As and electron transfer to As (i.e., hole transfer to Fe). In contrast, only little changes in the intensity of the prepeak are observed in the case of the Co substitution to Fe site.

Temperature dependences of the PFY-XAS spectra of $BaFe_2As_2$, $Ba(Fe_{0.92}Co_{0.08})_2As_2$, and $Ba_{0.6}K_{0.4}Fe_2As_2$ are shown in Fig. 7. Temperature-induced change in the electronic structure is small for all compounds here. Additionally, the energy of the absorption edge in Fig. 7(d) does not show a significant temperature dependence.

We also measured the pressure dependence of the PFY-XAS spectra of $BaFe_2As_2$, $Ba(Fe_{0.92}Co_{0.08})_2As_2$, and

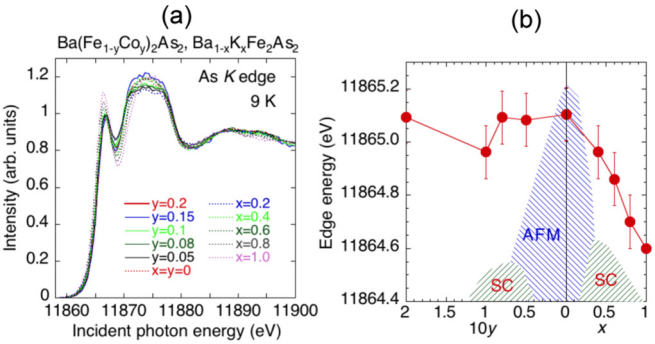

FIG. 6. (a) Chemical composition dependence of the PFY-XAS spectra of $Ba(Fe_{1-y}Co_y)_2As_2$ and $Ba_{1-x}K_xFe_2As_2$ at the As K-absorption edge. (b) Chemical composition dependence of the absorption edge energy. A schematic figure of two superconducting and AFM regions are also shown, where the full vertical scale corresponds to 150 K [21,23].

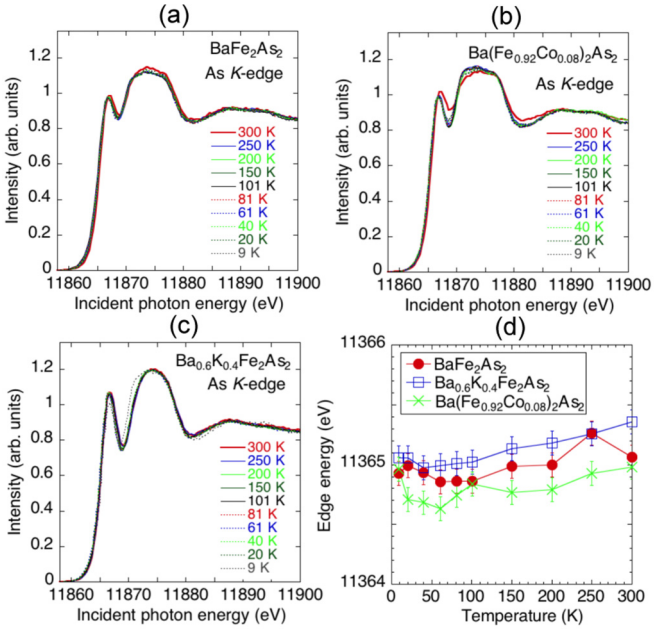

FIG. 7. Temperature dependence of the PFY-XAS spectra of (a) $BaFe_2As_2$, (b) $Ba(Fe_{0.92}Co_{0.08}y)_2As_2$, and (c) $Ba_{0.6}K_{0.4}Fe_2As_2$ at the As *K*-absorption edge. Temperature dependence of the absorption edge energy is also shown in (d).

$Ba_{0.6}K_{0.4}Fe_2As_2$ at 300 K as shown in Fig. 8. The intensity of the prepeak shows a discontinuous increase at 0.6 GPa for $BaFe_2As_2$, at 0.6 GPa for $Ba(Fe_{0.92}Co_{0.08})_2As_2$, and at 1.9 GPa for $Ba_{0.6}K_{0.4}Fe_2As_2$. While it increases monotonically in $Ba(Fe_{0.92}Co_{0.08})_2As_2$ with pressure, the shift of the As *K*

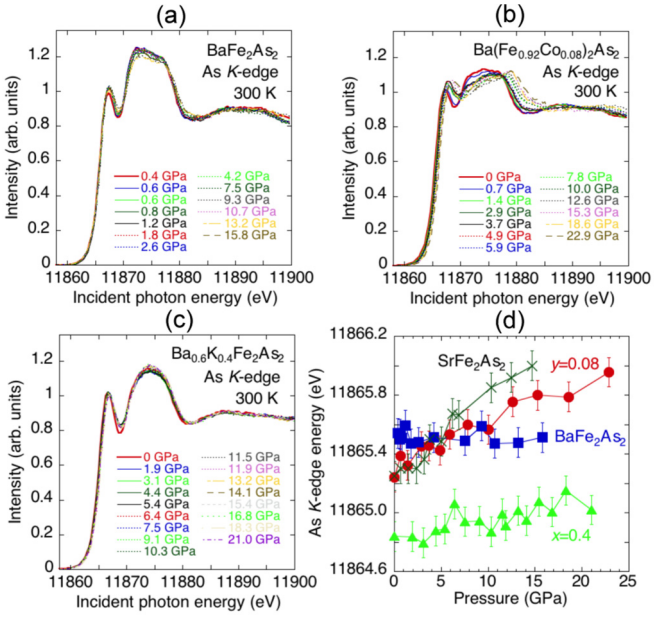

FIG. 8. Pressure dependence of the PFY-XAS spectra of (a) $BaFe_2As_2$, (b) $Ba(Fe_{0.92}Co_{0.08})_2As_2$, and (c) $Ba_{0.6}K_{0.4}Fe_2As_2$ at the As *K*-absorption edge and 300 K. Pressure dependence of the absorption edge energy of these compounds is also shown in (d) with the result of $SrFe_2As_2$.

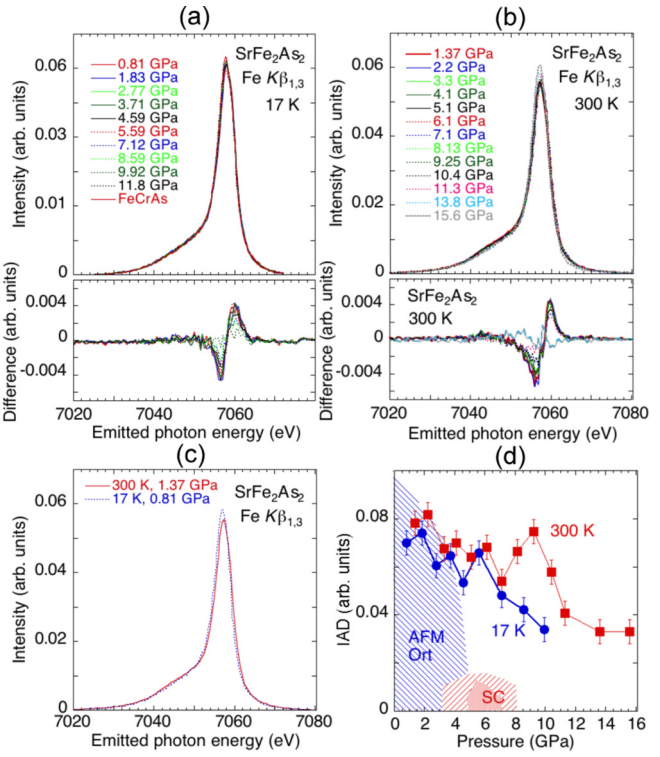

FIG. 9. Pressure dependence of the $K\beta$ XES spectra of $SrFe_2As_2$ (a) at 17 K and (b) at 300 K, with the difference for the spectrum at 17 K and 11.8 GPa (lower panels of each figure). (c) Comparison of the $K\beta$ XES spectra at 17 K and 0.81 GPa and at 300 K and 1.37 GPa. (d) Pressure dependence of the IAD values at 17 and 300 K. A schematic figure of superconducting and AFM regions (blue-colored area) are also shown, where the full vertical scale corresponds to 200 K [30]. A pale-red and a deep-red colored areas of the SC regions correspond to the filamentary and bulk superconductivity, respectively.

edge energy does not show significant pressure dependence for $BaFe_2As_2$ and $Ba_{0.6}K_{0.4}Fe_2As_2$.

B. $SrFe_2As_2$

1. Fe $K\beta$ XES

The $K\beta$ XES spectra were measured for a sister compound of $SrFe_2As_2$. Figures 9(a) and 9(b) show pressure dependence of the $K\beta$ XES spectra of $SrFe_2As_2$ at 17 K and at 300 K, respectively. The difference of the intensity for the spectrum at 17 K and 11.8 GPa is also shown. Figure 9(c) shows a comparison of the spectra at 17 and 300 K at low pressures. This suggests the same trend as observed in $BaFe_2As_2$, the change in the spin state to lower-spin state at low temperatures. The IAD values as a function of pressure are shown in Fig. 9(d). They show a monotonic decrease at both 17 and 300 K. The IAD values at 17 K are always lower than those at 300 K. The results of $SrFe_2As_2$ are similar to those of $BaFe_2As_2$.

2. PFY-XAS at Fe K-absorption edge

Pressure dependence of the pre-edge part of the PFY-XAS spectra of $SrFe_2As_2$ is measured at 17 K and 300 K, as shown in Figs. 10(a) and 10(b). We did not measure the spectra at the

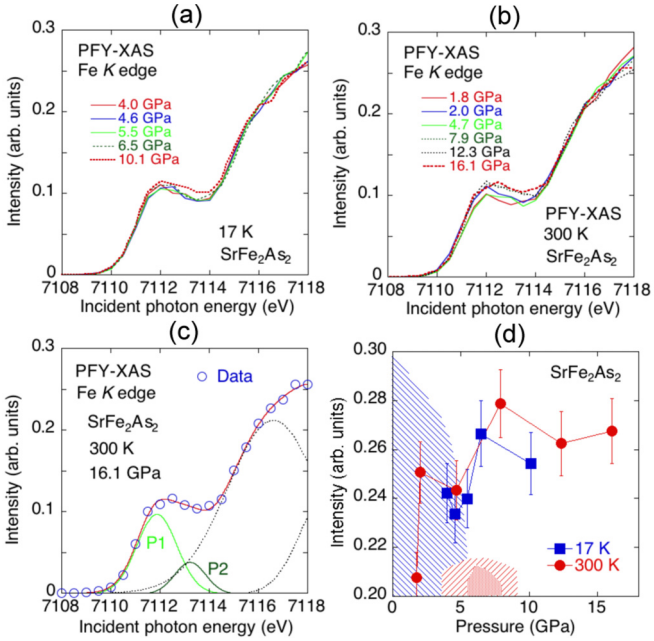

FIG. 10. Pressure dependence of the pre-edge part of the PFY-XAS spectra of $SrFe_2As_2$ (a) at 17 K and (b) at 300 K. (c) A fit example of the pre-edge part of the PFY-XAS spectra at 300 K and 16.1 GPa. (d) Pressure dependence of the pre-edge peak intensity (P1+P2) at 17 and 300 K. A schematic figure of superconducting and AFM regions are also shown in (d), where the full vertical scale corresponds to 200 K [30].

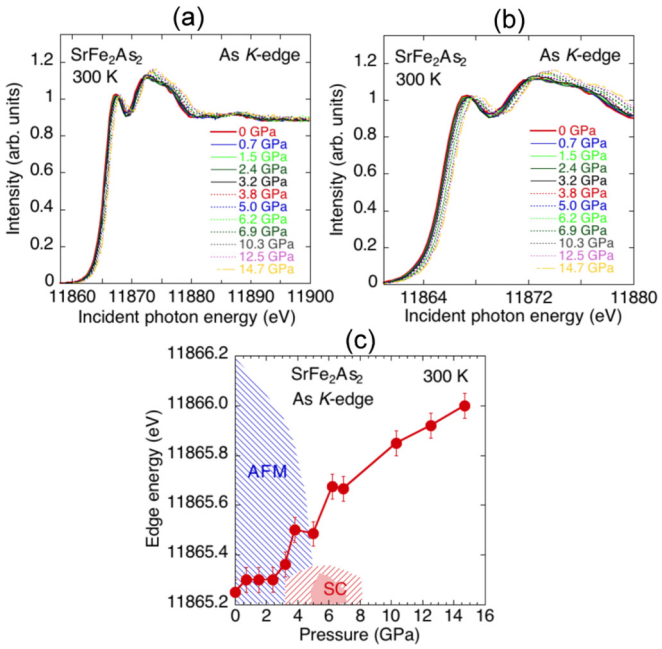

FIG. 11. (a) Pressure dependence of the PFY-XAS spectra of $SrFe_2As_2$ at As K-absorption edge and 300 K. (b) Expanded view around the absorption edge. (c) Pressure dependence of the absorption edge energy of $SrFe_2As_2$ (closed circles). A schematic figure of superconducting and AFM regions are also shown, where the full vertical scale corresponds to 200 K [30].

incident energy above the absorption edge and the intensity is normalized by the area of 7115–7117 eV. A fit example is shown in Fig. 10(c). Pressure dependence of the pre-edge peak intensity at 17 and 300 K is shown in Fig. 10(d). The pressure dependence of the total intensity of the pre-edge peak at 300 K shows a trend to increase with pressure.

3. *PFY-XAS at As K-absorption edge*

We show the pressure dependence of the PFY-XAS spectra of $SrFe_2As_2$ at the As K-absorption edge and 300 K in Fig. 11. The spectra shift to higher energy with pressure, almost keeping the shape, and the energy of the absorption energy shifts monotonically with pressure as shown in Fig. 11(d). This indicates the increase of the charge state of As and the electron transfer from As to other atoms with pressure. Seemingly, there are sudden increases of the electron transfer around the pressures of 3 and 5 GPa where the filamentary superconductivity and bulk superconductivity start, respectively.

IV. DISCUSSION

In these Fe122 superconductors there are common features: the decrease of the temperature induces the structural phase transition from tetragonal with C_4 symmetry to orthorhombic phase with C_2 symmetry. Parent compounds of $BaFe_2As_2$ and $SrFe_2As_2$ do not show the superconductivity, while both doping and pressure induces the superconductivity at low temperatures. At room temperature the pressure causes the T $\rightarrow$ cT isostructural transition and at low temperatures it breaks the C_2 symmetry of the orthorhombic phase with pressure. The As-As distance decreased rapidly with pressure and changed slowly in the cT phase, while the K doping $BaFe_2As_2$ served the same role of applying negative pressure along the c axis.

A. IAD values, local magnetic moment, and electron-electron correlation

In the doped samples of $BaFe_2As_2$ the temperature also decreases the IAD values and magnetic moment gradually. Such temperature dependence of the IAD values has been observed in the other 122-type iron-superconductor systems of $Ca_{1-x}RE_xFe_2As_2$ (RE = Pr and Nd) (Ref. [37]) and $Ca_{0.67}Sr_{0.33}Fe_2As_2$ (Ref. [16]) and explained later by the theory based on first-principles calculations with scaled magnetic interaction [49].

In the nondoped parent compounds the ordered magnetic moment is much smaller than the local moment [50,51]. It has been suggested theoretically that spatial and temporal quantum fluctuation of the local magnetic moment reduced the ordered moment significantly [10,52]. The theory suggested that the nesting contributes the fluctuation of the local magnetic moment. The local magnetic moment is caused by the electron-electron correlation through the Coulomb interaction. In this scenario the Co doping may cause the increase of the local magnetic moment because the doping reduces the nesting condition [53]. In iron-based superconductors it is known that the IAD values are proportional to the local magnetic moments [36,37]. In our results both the Co and K doping show a trend to increase the IAD values, i.e., the magnetic moment, supporting the above scenario.

Another theory suggested that the spin state of Fe controls the As-As bonding and the lattice parameters in $CaFe_2As_2$ [19,54]. The theory indicated that the local magnetic moment of Fe decreases with pressure, weakening the strength of the As-Fe bond, increasing the As-As interactions, and causing significant reduction in the c axis. This phenomenon has been observed as the T → cT phase transition experimentally, which has often occurred in the Fe-122 superconductors as described above. Pressure decreases the interlayer As-As distance, reaching close to the As-As covalent bond state at the cT phase. The theory indicated that the increase of the As-As bond strength in the cT phase weakens the correlation and decreases the local moment [19]. Experimentally pressure also suppresses the long-range AFM order as well as the local magnetic moment through the increase of the Fe $3d$–As $4p$ hybridization as described below. It is noted that the pressure dose not suppress the local magnetic moment completely in both $BaFe_2As_2$ and $SrFe_2As_2$, and the magnetic moment is partially reduced. In $BaFe_2As_2$ and $SrFe_2As_2$ the superconductivity disappeared at the cT phase. Our results show that the pressure decreased the IAD values, the magnetic moment, and thus the electron-electron correlation monotonically. These results may suggest that there is an optimum strength of Fe-spin state that is required for high-T_c superconductivity [19] and the electron-electron correlation may correlate to T_c.

It is known that the electron-electron correlation and the magnetic moment increase with the increasing pnictogen height (h) from FeAs layer in the order of LaFePO < LaFeAsO < $BaFe_2As_2$ < FeSe < FeTe [6]. The Fe $3d$–As $4p$ hybridization decreases with increasing h and the bond between Fe and As changes from covalent bond to ionic bond. In FeSe the electron-electron correlation is strong and no long-range magnetic order has been observed. However, the theory suggested that the orbital order and fluctuation originated from the nematicity and the nematic orbital fluctuations considered to play important roles in the pairing mechanism [55,56]. It was indicated that the origin of the electronic nematic state in Fe-based superconductors is the electron-electron correlation. Pressure decreases the pnictogen height and the electron-electron correlation in Fe122 superconductors. Thus the electron-electron correlation is considered to play an important role in the superconductivity.

Density functional calculations reproduced the pressure dependence of the volume and the transition to the cT phase in $BaFe_2As_2$ (Ref. [18]) and $SrFe_2As_2$ (Ref. [57]). The theory predicted the transition to the zero-magnetic moment at the cT phase [18,57]. We measured the pressure dependence of the Fe $K\beta$ emission spectra for $SrFe_2As_2$, from which we know the pressure-induced change in the IAD values, corresponding to the magnetic moment. The results indicate a gradual decrease of the magnetic moment with pressure up to 11.8 GPa at 17 K and up to 15.6 GPa at 300 K. A similar trend has been observed in $K_xFe_{2-y}Se_2$ [43]. Thus pressure-induced sudden disappearance of the magnetic moment at the cT phase is not likely in the Ba122 and Sr122 systems.

In $SrFe_2As_2$ pressure decreases the IAD values monotonically at 17 K in $SrFe_2As_2$, while it seems to show an anomaly around 7–11 GPa at 300 K as shown in Fig. 9(d). In $K_xFe_{2-y}Se_2$ the pressure-induced change in the IAD values at 300 K is gentle above the pressure of the T → cT structural transition [43]. Therefore, the pressure-induced anomaly of the IAD values at 300 K in $SrFe_2As_2$ possibly correlates to the T → cT structural transition at room temperature. In $SrFe_2As_2$ a structural transition from orthorhombic to tetragonal phase occurred around 4–5 GPa at 13 K [31]; however, the lattice parameter of c monotonically decreased in contrast to the T → cT transition at room temperature. The monotonic decrease of the IAD values at 17 K may also correspond to this gentle structural transition at 13 K. In $K_xFe_{2-y}Se_2$ a second SC dome was observed at cT phase, where the superconducting symmetry is considered to be different from the first SC dome, while in $SrFe_2As_2$ superconductivity seems to be suppressed at the cT phase.

Thus we can conclude that the Fe $3d$–As $4p$ hybridization plays a key role in suppressing the AFM order by the doping or pressure and it is reasonable to consider that the fluctuation of the local magnetic moment and the electron-electron correlation may also play a role in the appearance of the superconductivity.

B. Pre-edge peak of the PFY-XAS spectra at Fe K edge

The previous XAS study at Fe $L_{2,3}$ absorption edge by Merz *et al.* showed the peak shift to the higher energy only for the case of the hole doping with the K substitution in $BaFe_2As_2$ [28]. The substitution of K to the Ba site means the hole doping at Fe $3d$-derived states at the Fermi level. On the other hand, little effect on the Fe $3d$-derived states was observed with the electron doping by the Co substitution to the Fe site in $BaFe_2As_2$ [28,58]. The XAS spectra at As $L_{2,3}$ absorption edge showed a change in the intensity of the As $4p$-derived pre-edge peak for the Co substitution and no change for the K substitution [28]. Additionally, in the electron doping by the Co substitution to the Fe site the Fe valency remained unaffected in $SrFe_2As_2$ [27]. A prominent role of the hybridization between (Fe,Co) $3d_{xy}, d_{xz}, d_{yz}$ orbitals and As $4s/4p$ states was suggested for the band structure in $A(Fe_{1-x}Co_x)_2As_2$. These results agree with our XAS results at the Fe and As K-absorption edges.

Pressure may decrease the Fe-As distance, resulting in an increase of the overlap between Fe and As orbitals and the Fe $3d$ and As $4p$ hybridization [26]. The pre-edge peak of the PFY-XAS spectra at Fe K-absorption edge corresponds to the forbidden quadrupole transition and the increase in the intensity of the pre-edge peak as a measure of the hybridization with p states. Therefore, our results indicate that the pressure induces the increase of the hybridization between Fe $3d$ and As $4p$ in both compounds of $BaFe_2As_2$ and $SrFe_2As_2$. The increase of the intensity of the pre-edge peak correlates to the decrease of the magnetic moment as described above [42]. Thus the IAD values correlate to the magnetic moment and decrease with pressure, which also corresponds well to the increase of the intensity of the pre-edge peak of the PFY-XAS spectra at the Fe K-absorption edge at high pressures.

Figure 10(d) suggests that in $SrFe_2As_2$ the pressure increases the d-p hybridization, corresponding to the decrease of the IAD values in Fig. 9(d) and thus the shift to the lower-spin state. Interestingly, the pressure-induced change in the pre-edge peak intensity seems to correlate to T_c.

C. PFY-XAS spectra at As K edge

Here, we consider the Fe $3d$–As $4p$ hybridization by summarizing the results of the XAS spectra at the Fe and As K-absorption edges. In $BaFe_2As_2$ the K substitution to the Ba site lowered the energy of the As K-absorption edge by increasing the intensity of the prepeak, while the Co substitution to the Fe site does not change the electronic structure, as shown in Fig. 6. These phenomena correspond well to the change in the lattice parameters in Fig. 2(d). The K substitution resulted in the decrease of the As valence. The K substitution also caused a slight shift of the energy of the Fe K-absorption edge to higher energy as shown in Fig. 4(a). A similar shift of the edge energy at the Fe L_3 absorption edge and the increase of the As-As distance by the K substitution were reported, although the Fe-As distance did not change [28]. These results confirm the hole doping from As to Fe sites by the K substitution with increasing the Fe-As hybridization, which was consistent with the results of the increase of the pre-edge peak of the XAS spectra at the Fe-K-absorption edge and that of the prepeak of the XAS spectra at the As K-absorption edge.

The Co or electron doping was insensitive to the change in both electronic structures at the Fe and As K-absorption edges as well as the lattice constants. However, the pre-edge peak intensity at the Fe K edge shows a trend of increase at higher doping level as shown in Figs. 4(a) and 4(d), although it is not clear at the SC region. Similar results have been reported that no Co-doping effect was observed at the Fe nor Co L-absorption edges in $Sr(Fe_{1-x}Co_x)_2As_2$ [27]. They concluded that the covalency of the (Fe,Co)-As bond was a key parameter for the interplay between magnetism and superconductivity. A small amount of Co doping, i.e., one additional electron, caused significant effect to suppress the AFM order, emerging the SC region. A recent theory using the the Hubbard model with the self-consistent vertex-correction method, which successfully explained the phase diagram and the superconductivity of the Fe-based superconductors in a unified way, may suggest a possible scenario [8,55,56]. The theory indicated that the spin + orbital fluctuation is a driving mechanism of the superconductivity in iron-based superconductors and it depends on the electron-electron correlation and Fermi surface structure such as the nesting condition. The Co doping may weaken the nesting condition with reducing the spin susceptibility and the AFM order may be suppressed. However, a detailed mechanism has not been clarified yet. Further theoretical investigation may be required.

The pressure dependence of the PFY-XAS spectra at the As K-absorption edge shows a discontinuous increase at 0.6 GPa for $BaFe_2As_2$ and $Ba(Fe_{0.92}Co_{0.08})_2As_2$ and at 1.9 GPa for $Ba_{0.6}K_{0.4}Fe_2As_2$. It is understandable that the critical transition pressure of $BaFe_2As_2$ is almost the same as that of $Ba(Fe_{0.92}Co_{0.08})_2As_2$ because the Co substitution did not show a significant effect crystallographically. However, the pressure-induced change in the electronic structure of $Ba(Fe_{0.92}Co_{0.08})_2As_2$ is more drastic compared to that of $BaFe_2As_2$ as shown in Fig. 8. A similar behavior was previously observed in $BaFe_2As_2$, where the critical pressure was approximately 1 GPa and the sudden increase of the prepeak intensity occurred at the Fe-As interatomic distance of 2.39 Å [26]. The pressure-induced shift of the As K-absorption edge was little as shown in Fig. 8(d) in $BaFe_2As_2$ and $Ba(Fe_{0.92}Co_{0.08})_2As_2$ in contrast to the results by Balédent *et al.* [26]. The pre-edge peak intensity at Fe K-absorption edge at 3 GPa increased compared to that at ambient pressure as shown in Figs. 4(b) and 4(d), also in contrast to the results reported by Balédent *et al.* [25]. These results lead to the similar conclusion discussed in the above subsection that pressure caused the increase of the Fe $3d$–As $4p$ hybridization, which resulted in the increase of the pre-edge peak intensity at the Fe K-absorption edge and the prepeak intensity at As K-absorption edge. It is noted that in $BaFe_2As_2$ and $Ba_{0.6}K_{0.4}Fe_2As_2$ the pressure-induced change in the electronic structure at the As K-absorption edge above the critical pressure is very small as shown in Figs. 8(a) and 8(c), and even at the SC region.

In $SrFe_2As_2$ the pressure induced a different behavior from the $BaFe_2As_2$ systems. There was no critical pressure to change the electronic structure abruptly and the As K-absorption edge shifts to higher energy continuously with pressure as shown in Fig. 11(c). This is similar to the shift in $Ba(Fe_{0.92}Co_{0.08})_2As_2$ in Fig. 8(d). The pressure works to dope the electrons from the As site to the Fe site in $SrFe_2As_2$ and $Ba(Fe_{0.92}Co_{0.08})_2As_2$. The intensity of the pre-edge peak at the Fe K-absorption edge may increase with pressure as shown in Fig. 10(d). While the pressure-induced change in the intensity of the prepeak at the As K-absorption edge was not observed as shown in Fig. 11(b), the shift of the As K-absorption edge occurred. These results suggest the electron transfer from As to Fe and the Fermi level shift to higher binding energy without the change in the electronic structure of As with pressure. In $SrFe_2As_2$ there was no critical pressure for the spectra at the As K-absorption edge in contrast to the Ba122 systems.

V. CONCLUSION

The electronic structures of electron- and hole-doped $BaFe_2As_2$ [$Ba_{1-x}K_xFe_2As_2$ and $Ba(Fe_{1-y}Co_y)_2As_2$] and $SrFe_2As_2$ were studied systematically by measuring the $K\beta$ XES and PFY-XAS at the Fe and As K-absorption edges as functions of the chemical composition and pressure. The IAD values of the Fe $K\beta$ spectra decreased with decreasing the temperature in $Ba_{1-x}K_xFe_2As_2$ and $Ba(Fe_{1-y}Co_y)_2As_2$. Both the electron and hole doping by the chemical substitutions increased the IAD values slightly, while the PFY-XAS spectra at the Fe K-absorption edge did not show a significant doping dependence. The hole doping with the K substitution and the pressure created the increase of the pre-edge peak intensity of the PFY-XAS spectra at the Fe K-absorption edge. This indicates the transition to the lower-spin state, i.e., smaller magnetic moment. Pressure induced the lower-spin states in $BaFe_2As_2$ and $SrFe_2As_2$, resulting in the smaller magnetic moment. However, the magnetic moment is partially reduced and the pressure did not suppress the local magnetic moment completely in both $BaFe_2As_2$ and $SrFe_2As_2$. In $SrFe_2As_2$ the magnetic moment and the electron-electron correlation decreased monotonically with pressure in the pressure range measured.

Both electronic structures at the Fe and As K-absorption edges as well as the lattice constants were insensitive to the electron doping with the Co substitution, while the PFY-XAS

spectra at the As K-absorption edge showed that in $BaFe_2As_2$ the K substitution to the Ba site lowered the energy of the As K-absorption edge with increasing the intensity of the prepeak. Thus the K substitution decreased the As valence. We found that in the PFY-XAS spectra at As K-absorption edge pressure induced a discontinuous increase of the prepeak intensity at 0.6 GPa for $BaFe_2As_2$ and $Ba(Fe_{0.92}Co_{0.08})_2As_2$, and at 1.9 GPa for $Ba_{0.6}K_{0.4}Fe_2As_2$, while in $SrFe_2As_2$ no critical pressure was observed. We, however, still do not understand the mechanism of the sudden change in the electronic structure at low pressures and its role on the superconductivity. The pressure did not change the energy of the As K-absorption edge in $BaFe_2As_2$ and $Ba_{0.6}K_{0.4}Fe_2As_2$. Meanwhile, the energy of the As K-absorption edge increased with pressure in $SrFe_2As_2$ and $Ba(Fe_{0.92}Co_{0.08})_2As_2$, indicating a pressure-induced electron doping to the Fe site.

Our results suggest that the Fe $3d$–As $4p$ hybridization plays a key role by suppressing the AFM order under pressure in the Fe122 superconductors. The electron doping is also effective in suppressing the AFM order and the emergence of the superconductivity without change in the lattice constants. The fluctuation of the local magnetic moment may also play a role on the physical properties of the iron superconductors and an optimum strength of Fe-spin state may exist for high T_c. The electron-electron correlation that connects to the magnetic moment and the pnictogen height may be also important for the emergence of the superconductivity in the Fe122 systems.

ACKNOWLEDGMENTS

The experiments were performed at Taiwan beamlines BL12XU and BL12B2 at SPring-8 under Proposals No. 2015A4254, No. 2015A4128, No. 2015B4262, No. 2016A4256, No. 2016B4262, and No. 2016B4134 (corresponding NSRRC Proposals No. 2015-2-034 and No. 2016-3-095), and 16-ID-D beamline of the APS, ANL. This work at SPring-8 is supported by Grants in Aid for Scientific Research from the Japan Society for the Promotion of Science, KAKENHI No. 15K05194. Portions of this work were performed at HPCAT (Sector16), Advanced Photon Source (APS), Argonne National Laboratory. HPCAT operation is supported by DOE-NNSA under Award No. DE-NA0001974, with partial instrumentation funding by NSF. The Advanced Photon Source is a US Department of Energy (DOE) Office of Science User Facility operated for the DOE Office of Science by Argonne National Laboratory under Contract No. DE-AC02-06CH11357. P.C. and Y.X. acknowledge the support of DOE-BES/DMSE under Award No. DE-FG02-99ER45775. Works at IOPCAS are supported by NSF and MOST of China through Research Projects, as well as by CAS External Cooperation Program of BIC (No. 112111KYS820150017). J.-F.L. acknowledges support from HPSTAR. We thank Seika Shonai for help in the experiments at SPring-8. We also appreciate Young-June Kim at the University of Toronto and Hlynur Gretarsson at Max Plank Institute for Solid State Research for the preparation of the FeCrAs sample.

[1] Y. Kamihara, T. Watanabe, M. Hirano, and H. Hosono, Iron-based layered superconductor $La[O_{1-x}F_x]FeAs$ ($x = 0.05$–0.12) with $T_c = 26$ K, J. Am. Chem. Soc. **130**, 3296 (2008).

[2] G. L. Stewart, Superconductivity in iron compounds, Rev. Mod. Phys. **83**, 1589 (2011).

[3] H. Hosono and K. Kuroki, Iron-based superconductors: Current status of materials and pairing mechanism, Physica C **514**, 399 (2015).

[4] C. H. Lee, A. Iyo, H. Eisaki, H. Kito, M. T. Fernandez-Diaz, T. Ito, K. Kihou, H. Matsuhata, M. Braden, and K. Yamada, Effect of structural parameters on superconductivity in fluorine-free $LnFeAsO_{1-y}$ (Ln = La, Nd), J. Phys. Soc. Jpn. **77**, 083704 (2008).

[5] K. Kuroki, H. Usui, S. Onari, R. Arita, and H. Aoki, Pnictogen height as a possible switch between high-T_c nodeless and low-T_c nodal pairings in the iron-based superconductors, Phys. Rev. B **79**, 224511 (2009).

[6] Y. Mizuguchi, Y. Hara, K. Deguchi, S. Tsuda, T. Yamaguchi, K. Takeda, H. Kotegawa, H. Tou, and Y. Takano, Anion height dependence of T_c for the Fe-based superconductor, Supercond. Sci. Technol. **23**, 054013 (2010).

[7] K. Deguchi, Y. Takano, and Y. Mizuguchi, Physics and chemistry of layered chalcogenide superconductors, Sci. Technol. Adv. Mater. **13**, 054303 (2012).

[8] S. Onari, Y. Yamakawa, and H. Kontani, High-T_c Superconductivity Near the Anion Height Instability in Fe-Based Superconductors: Analysis of $LaFeAsO_{1-x}H_x$, Phys. Rev. Lett. **112**, 187001 (2014).

[9] P. Dai, Antiferromagnetic order and spin dynamics in iron-based superconductors, Rev. Mod. Phys. **87**, 855 (2015).

[10] Y.-T. Tam, D.-X. Yao, and W. Ku, Itinerancy-enhanced Quantum Fluctuation of Magnetic Moments in Iron-based Superconductors, Phys. Rev. Lett. **115**, 117001 (2015).

[11] A. Kreyssig, M. A. Green, Y. Lee, G. D. Samolyuk, P. Zajdel, J. W. Lynn, S. L. Bud'ko, M. S. Torikachvili, N. Ni, S. Nandi, J. B. Leão, S. J. Poulton, D. N. Argyriou, B. N. Harmon, R. J. McQueeney, P. C. Canfield, and A. I. Goldman, Pressure-induced volume-collapsed tetragonal phase of $CaFe_2As_2$ as seen via neutron scattering, Phys. Rev. B **78**, 184517 (2008).

[12] W. Uhoya, G. Tsoi, Y. K. Vohra, M. A. McGuire, A. S. Sefat, B. C. Sales, D. Mandrus, and S. T. Weir, Anomalous compressibility effects and superconductivity of $EuFe_2As_2$ under high pressures, J. Phys.: Condens. Matter **22**, 292202 (2010).

[13] W. Uhoya, A. Stemshorn, G. Tsoi, Y. K. Vohra, A. S. Sefat, B. C. Sales, K. M. Hope, and S. T. Weir, Collapsed tetragonal phase and superconductivity of $BaFe_2As_2$ under high pressure, Phys. Rev. B **82**, 144118 (2010).

[14] R. Mittal, S. K. Mishra, S. L. Chaplot, S. V. Ovsyannikov, E. Greenberg, D. M. Trots, L. Dubrovinsky, Y. Su, Th. Brueckel, S. Matsuishi, H. Hosono, and G. Garbarino, Ambient- and low-temperature synchrotron x-ray diffraction study of $BaFe_2As_2$ and $CaFe_2As_2$ at high pressures up to 56 GPa, Phys. Rev. B **83**, 054503 (2011).

[15] W. O. Uhoya, J. M. Montgomery, G. M. Tsoi, Y. K. Vohra, M. A. McGuire, A. S. Sefat, B. C. Sales, and S. T. Weir, Phase transition and superconductivity of $SrFe_2As_2$ under high pressure, J. Phys.: Condens. Matter **23**, 122201 (2011).

[16] J. R. Jeffries, N. P. Butch, M. J. Lipp, J. A. Bradley, K. Kirshenbaum, S. R. Saha, J. Paglione, C. Kenney-Benson,

Y. Xiao, P. Chow, and W. J. Evans, Persistent Fe moments in the normal-state collapsed-tetragonal phase of the pressure-induced superconductor $Ca_{0.67}Sr_{0.33}Fe_2Fe_2$, Phys. Rev. B **90**, 144506 (2014).

[17] E. Stavrou, X.-J. Chen, A. R. Oganov, A. F. Wang, Y. J. Yan, X. G. Luo, X. H. Chen, and A. F. Goncharov, Formation of As-As interlayer bonding in the collapsed tetragonal phase of $NaFe_2As_2$ under pressure, Sci. Rep. **5**, 9868 (2015).

[18] N. Colonna, G. Profeta, Al. Continenza, and S. Massidda, Structural and magnetic properties of $CaFe_2As_2$ and $BaFe_2As_2$ from first-principles density functional theory, Phys. Rev. B **83**, 094529 (2011).

[19] T. Yildirim, Strong Coupling of the Fe-spin State and the As-As Hybridization in Iron-pnictide Superconductors from First-principle Calculations, Phys. Rev. Lett. **102**, 037003 (2009).

[20] A. Sanna, G. Profeta, S. Massidda, and E. K. U. Gross, First-principles study of rare-earth-doped superconducting $CaFe_2As_2$, Phys. Rev. B **86**, 014507 (2012).

[21] N. Ni, M. E. Tillman, J.-Q. Yan, A. Kracher, S. T. Hannahs, S. L. Bud'ko, and P. C. Canfield, Effects of Co substitution on thermodynamic and transport properties and anisotropic H_{c2} in $Ba(Fe_{1-x}Co_x)_2As_2$ single crystals, Phys. Rev. B **78**, 214515 (2008).

[22] S. Avci, O. Chmaissem, E. A. Goremychkin, S. Rosenkranz, J.-P. Castellan, D. Y. Chung, I. S. Todorov, J. A. Schlueter, H. Claus, M. G. Kanatzidis, A. Daoud-Aladine, D. Khalyavin, and R. Osborn, Magnetoelastic coupling in the phase diagram of $Ba_{1-x}K_xFe_2As_2$ as seen via neutron diffraction, Phys. Rev. B **83**, 172503 (2011).

[23] M. Rotter, M. Pangerl, M. Tegel, and D. Johrendt, Superconductivity and crystal structures of $(Ba_{1-x}K_xFe_2As_2$ ($x = 0$–1), Angew. Chem. Int. Ed. **47**, 7949 (2008).

[24] J. Wu, J.-F. Lin, X. C. Wang, Q. Q. Liu, J. L. Zhu, Y. M. Xiac, P. Chow, and C. Jina, Pressure-decoupled magnetic and structural transitions of the parent compound of iron-based 122 superconductors, $BaFe_2As_2$, Proc. Natl. Acad. Sci. USA **110**, 17263 (2013).

[25] V. Balédent, F. Rullier-Albenque, D. Colson G. Monaco, and J.-P. Rueff, Stability of the Fe electronic structure through temperature-, doping-, and pressure-induced transitions in the $BaFe_2As_2$ superconductors, Phys. Rev. B **86**, 235123 (2012).

[26] V. Balédent, F. Rullier-Albenque, D. Colson, J. M. Ablett, and J.-P. Rueff, Electronic Properties of $BaFe_2As_2$ Upon Doping and Pressure: The Prominent Role of the As p Orbitals, Phys. Rev. Lett. **114**, 177001 (2015); we note that the absolute energy scale of the incident photon energy in the XAS spectra at As-K absorption edge may be wrong in this paper.

[27] M. Merz, F. Eilers, Th. Wolf, P. Nagel, H. v. Löhneysen, and S. Schuppler, Electronic structure of single-crystalline $Sr(Fe_{1-x}Co_x)_2As_2$ probed by x-ray absorption spectroscopy: Evidence for effectively isovalent substitution of Fe^{2+} by Co^{2+}, Phys. Rev. B **86**, 104503 (2012).

[28] M. Merz, P. Schweiss, P. Nagel, M.-J. Huang, R. Eder, T. Wolf, H. von Löhneysen, and S. Schuppler, Of substitution and doping: Spatial and electronic structure in Fe pnictides, J. Phys. Soc. Jpn. **85**, 044707 (2016).

[29] H. Kotegawa, H. Sugawara, and H. Tou, Abrupt emergence of pressure-induced superconductivity of 34 K in $SrFe_2As_2$: A resistivity study under pressure, J. Phys. Soc. Jpn. **78**, 013709 (2009).

[30] K. Matsubayashi, N. Katayama, K. Ohgushi, A. Yamada, K. Munakata, T. Matsumoto, and Y. Uwatoko, Intrinsic properties of AFe_2As_2 (A = Ba, Sr) single crystal under highly hydrostatic pressure conditions, J. Phys. Soc. Jpn. **78**, 073706 (2009).

[31] J. J. Wu, J. F. Lin, X. C. Wang, Q. Q. Liu, J. L. Zhu, Y. M. Xiao, P. Chow, and C. Q. Jin, Magnetic and structural transitions of $SrFe_2As_2$ at high pressure and low temperature, Sci. Rep. **4**, 3685 (2014).

[32] Y. Q. Wang, P. C. Lu, J. J. Wu, J. Liu, X. C. Wang, J. Y. Zhao, W. L. Bi, E. E. Alp, C. Y. Park, D. Popov, C. Q. Jin, J. Sun, and J. F. Lin, Phonon density of states of single-crystal $SrFe_2As_2$ across the collapsed phase transition at high pressure, Phys. Rev. B **94**, 014516 (2016).

[33] K. Tsutsumi, The x-ray non-diagram lines $K\beta$ of some compounds of the iron group, J. Phys. Soc. Jpn. **14**, 1696 (1959).

[34] K. Tsutsumi, H. Nakamori, and K. Ichikawa, x-ray Mn $K\beta$ emission spectra of manganese oxides and manganates, Phys. Rev. B **13**, 929 (1976).

[35] G. Vankó, T. Neisius, G. Molnár, F. Renz, S. Kárpáti, A. Shukla, and F. M. F. de Groot, Probing the 3d spin momentum with x-ray emission spectroscopy: The case of molecular-spin transitions, J. Phys. Chem. B **110**, 11647 (2006).

[36] H. Gretarsson, A. Lupascu, Jungho Kim, D. Casa, T. Gog, W. Wu, S. R. Julian, Z. J. Xu, J. S. Wen, G. D. Gu, R. H. Yuan, Z. G. Chen, N.-L. Wang, S. Khim, K. H. Kim, M. Ishikado, I. Jarrige, S. Shamoto, J.-H. Chu, I. R. Fisher, and Y.-J. Kim, Revealing the dual nature of magnetism in iron pnictides and iron chalcogenides using x-ray emission spectroscopy, Phys. Rev. B **84**, 100509 (2011).

[37] H. Gretarsson, S. R. Saha, T. Drye, J. Paglione, Jungho Kim, D. Casa, T. Gog, W. Wu, S. R. Julian, and Y.-J. Kim, Spin-State Transition in the Fe Pnictides, Phys. Rev. Lett. **110**, 047003 (2013).

[38] J.-P. Rueff and A. Shukla, Inelastic x-ray scattering by electronic excitations under high pressure, Rev. Mod. Phys. **82**, 847 (2010).

[39] K. Hämäläinen, D. P. Siddons, J. B. Hastings, and L. E. Berman, Elimination of the Inner-shell Lifetime Broadening in x-ray-Absorption Spectroscopy, Phys. Rev. Lett. **67**, 2850 (1991).

[40] K. Hämäläinen, C. C. Kao, J. B. Hasting, D. P. Siddons, L. E. Berman, V. Stojanoff, and S. P. Cramer, Spin-dependent x-ray absorption of MnO and MnF_2, Phys. Rev. B **46**, 14274 (1992).

[41] K. Zhao, Q. Q. Liu, X. C. Wang, Z. Deng, Y. X. Lv, J. L. Zhu, F. Y. Li, and C. Q. Jin, Superconductivity above 33 K in $(Ca_{1-x}Na_xFe_2As_2$, J. Phys.: Condens. Matter **22**, 222203 (2016).

[42] H. Yamaoka, Pressure dependence of the electronic structure of 4f and 3d electron systems studied by x-ray emission spectroscopy, High Press. Res. **36**, 262 (2016).

[43] Y. Yamamoto, H. Yamaoka, M. Tanaka, H. Okazaki, T. Ozaki, Y. Takano, J.-F. Lin, H. Fujita, T. Kagayama, K. Shimizu, N. Hiraoka, H. Ishii, K.-D. Tsuei, and J. Mizuki, Origin of pressure-induced superconducting phase in $K_xFe_{2-y}Se_2$ studied by synchrotron x-ray diffraction and spectroscopy, Sci. Rep. **6**, 30946 (2016).

[44] H.-K. Mao and P. M. Bell, High-pressure physics: The 1-megabar mark on the ruby $R1$ static pressure scale, Science **191**, 851 (1976).

[45] K. Syassen, Ruby under pressure, High Press. Res. **28**, 75 (2008).

[46] H. Yamaoka, Y. Zekko, I. Jarrige, J.-F. Lin, N. Hiraoka, H. Ishii, K.-D. Tsuei, and J. Mizuki, Ruby pressure scale in a low-temperature diamond anvil cell, J. Appl. Phys. **112**, 124503 (2012).

[47] J. M. Chen, S. C. Haw, J. M. Lee, T. L. Chou, S. A. Chen, K. T. Lu, Y. C. Liang, Y. C. Lee, N. Hiraoka, H. Ishii, K. D. Tsuei, E. Huang, and T. J. Yang, Pressure dependence of the electronic structure and spin state in $Fe_{1.01}Se$ superconductors probed by x-ray absorption and x-ray emission spectroscopy, Phys. Rev. B **84**, 125117 (2011).

[48] L. Simonelli, N. L. Saini, M. Moretti Sala, Y. Mizuguchi, Y. Takano, H. Takeya, T. Mizokawa, and G. Monaco, Coexistence of different electronic phases in the $K_{0.8}Fe_{1.6}Se_2$ superconductor: A bulk-sensitive hard x-ray spectroscopy study, Phys. Rev. B **85**, 224510 (2012).

[49] L. Ortenzi, H. Gretarsson, S. Kasahara, Y. Matsuda, T. Shibauchi, K. D. Finkelstein, W. Wu, S. R. Julian, Y.-J. Kim, I. I. Mazin, and L. Boeri, Structural Origin of the Anomalous Temperature Dependence of the Local Magnetic Moments in the $CaFe_2As_2$ Family of Materials, Phys. Rev. Lett. **114**, 047001 (2015).

[50] Q. Huang, Y. Qiu, Wei Bao, M. A. Green, J. W. Lynn, Y. C. Gasparovic, T. Wu, G. Wu, and X. H. Chen, Neutron-diffraction Measurements of Magnetic Order and a Structural Transition in Parent $BaFe_2As_2$ Compound of FeAs-based High-temperature Superconductors, Phys. Rev. Lett. **101**, 257003 (2008).

[51] Z. P. Yin, K. Haule, and G. Kotliar, Kinetic frustration and the nature of the magnetic and paramagnetic states in iron pnictides and iron chalcogenides, Nat. Mater. **10**, 932 (2011).

[52] Q. Si and E. Abrahams, Strong Correlations and Magnetic Frustration in the High T_c Iron Pnictides, Phys. Rev. Lett. **101**, 076401 (2008).

[53] K. Terashima, Y. Sekiba, J. H. Bowen, K. Nakayama, T. Kawahara, T. Sato, P. Richard, Y.-M. Xu, L. J. Li, G. H. Cao, Z.-A. Xu, H. Ding, and T. Takahashi, Fermi surface nesting induced strong pairing in iron-based superconductors, PNAS (USA) **106**, 7330 (2009).

[54] R. Yang, C. Le, L. Zhang, B. Xu, W. Zhang, K. Nadeem, H. Xiao, J. Hu, and X. Qiu, Formation of As-As bond and its effect on absence of superconductivity in the collapsed tetragonal phase of $Ca_{0.86}Pr_{0.14}Fe_2As_2$: An optical spectroscopy study, Phys. Rev. B **91**, 224507 (2015).

[55] S. Onari, Y. Yamakawa, and H. Kontani, Sign-reversing Orbital Polarization in the Nematic Phase of FeSe Due to the C_2 Symmetry Breaking in the Self-energy, Phys. Rev. Lett. **116**, 227001 (2016).

[56] Y. Yamakawa, S. Onari, and H. Kontani, Nematicity and Magnetism in FeSe and Other Families of Fe-based Superconductors, Phys. Rev. X **6**, 021032 (2016).

[57] K. F. Quader and M. Widom, Pressure-driven enthalpic and Lifshitz transition in 122-Pnictides, Contrib. Plasma Phys. **55**, 128 (2015).

[58] E. M. Bittar, C. Adriano, T. M. Garitezi, P. F. S. Rosa, L. Mendonça-Ferreira, F. Garcia, G. de, M. Azevedo, P. G. Pagliuso, and E. Granado, Co-substitution Effects on the Fe Valence in the $BaFe_2As_2$ Superconducting Compound: A Study of Hard x-ray Absorption Spectroscopy, Phys. Rev. Lett. **107**, 267402 (2011).